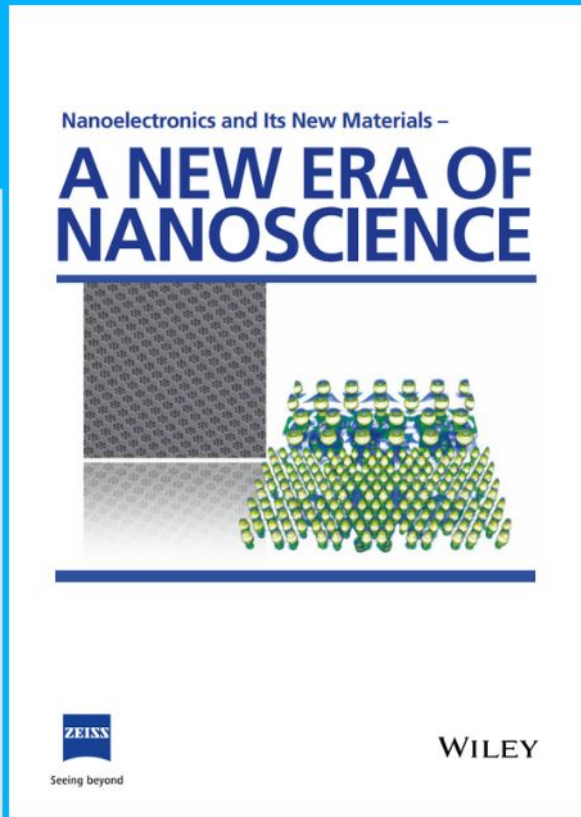




# Nanoelectronics and Its New Materials – A NEW ERA OF NANOSCIENCE



**Discover the recent advances in electronics research and fundamental nanoscience.**

Nanotechnology has become the driving force behind breakthroughs in engineering, materials science, physics, chemistry, and biological sciences. In this compendium, we delve into a wide range of novel applications that highlight recent advances in electronics research and fundamental nanoscience. From surface analysis and defect detection to tailored optical functionality and transparent nanowire electrodes, this eBook covers key topics that will revolutionize the future of electronics.

To get your hands on this valuable resource and unleash the power of nanotechnology, simply download the eBook now. Stay ahead of the curve and embrace the future of electronics with nanoscience as your guide.



Seeing beyond

**WILEY**

# Graphene-Nanorod Enhanced Quasi-Van Der Waals Epitaxy for High Indium Composition Nitride Films

Shuo Zhang, Bingyao Liu, Fang Ren, Yue Yin, Yunyu Wang, Zhaolong Chen, Bei Jiang, Bingzhi Liu, Zhetong Liu, Jingyu Sun, Meng Liang, Jianchang Yan, Tongbo Wei, Xiaoyan Yi,\* Junxi Wang, Jinmin Li, Peng Gao,\* Zhongfan Liu,\* and Zhiqiang Liu\*

The nitride films with high indium (In) composition play a crucial role in the fabrication of In-rich InGaN-based optoelectronic devices. However, a major limitation is In incorporation requiring a low temperature during growth at the expense of nitride dissociation. Here, to overcome this limitation, a strain-modulated growth method, namely the graphene (Gr)-nanorod (NR) enhanced quasi-van der Waals epitaxy, is proposed to increase the In composition in InGaN alloy. The lattice transparency of Gr enables constraint of in-plane orientation of nitride film and epitaxial relationships at the heterointerface. The Gr interlayer together with NRs buffer layer substantially reduces the stress of the GaN film by 74.4%, from 0.9 to 0.23 GPa, and thus increases the In incorporation by 30.7%. The first principles calculations confirm that the release of strain accounts for the dramatic improvement. The photoluminescence peak of multiple quantum wells shifts from 461 to 497 nm and the functionally small-sized cyan light-emitting diodes of  $7 \times 9 \text{ mil}^2$  are demonstrated. These findings provide an efficient approach for the growth of In-rich InGaN film and extend the applications of nitrides in advanced optoelectronic, photovoltaic, and thermoelectric devices.

## 1. Introduction


Over the past few years, nitrides, specifically GaN and Ga-rich InGaN, are proven to be the most important and indispensable materials for the fabrication of light emitters in the blue and near ultraviolet spectral regions.<sup>[1,2]</sup> Due to the bandgap tunability of InGaN alloy system, there also has been extensive research to extend the applications of indium (In)-rich InGaN-based semiconductor devices such as full-color displays, high-efficiency photovoltaic solar cells, fiber optics, and thermoelectric and nonlinear optical devices,<sup>[3–8]</sup> in which the GaN is commonly used as the template to grow In-rich InGaN films. However, the development of nitride films with high In composition remains challenging in terms of phase separation, InN decomposition, and relatively high vapor pressure.<sup>[9,10]</sup> These limitations could be

S. Zhang, F. Ren, Y. Yin, Dr. Y. Y. Wang, Dr. M. Liang, Prof. J. C. Yan, Prof. T. B. Wei, Prof. X. Y. Yi, Prof. J. X. Wang, Prof. J. M. Li, Prof. Z. Q. Liu  
Research and Development Center for Semiconductor  
Lighting Technology  
Institute of Semiconductors  
Chinese Academy of Sciences  
Beijing 100083, China  
E-mail: spring@semi.ac.cn; lzq@semi.ac.cn

S. Zhang, F. Ren, Y. Yin, Dr. Y. Y. Wang, Dr. M. Liang, Prof. J. C. Yan, Prof. T. B. Wei, Prof. X. Y. Yi, Prof. J. X. Wang, Prof. J. M. Li, Prof. Z. Q. Liu  
Center of Materials Science and Optoelectronics Engineering  
University of Chinese Academy of Sciences  
Beijing 100049, China

B. Y. Liu, Z. T. Liu, Prof. P. Gao  
Electron Microscopy Laboratory and International Center  
for Quantum Materials, School of Physics  
Peking University  
Beijing 100871, China  
E-mail: p-gao@pku.edu.cn

B. Y. Liu, Z. T. Liu, Prof. P. Gao  
Academy for Advanced Interdisciplinary Studies  
Peking University  
Beijing 100871, China

 The ORCID identification number(s) for the author(s) of this article can be found under <https://doi.org/10.1002/smll.202100098>.

B. Y. Liu, Dr. Z. L. Chen, B. Jiang, B. Z. Liu, Z. T. Liu, Prof. Z. F. Liu  
Center for Nanochemistry (CNC)  
Beijing Science and Engineering Center for Nanocarbons  
Beijing National Laboratory for Molecular Sciences  
College of Chemistry and Molecular Engineering  
Peking University  
Beijing 100871, China  
E-mail: zfliu@pku.edu.cn

B. Y. Liu, Dr. Z. L. Chen, B. Z. Liu, Z. T. Liu, Prof. J. Y. Sun, Prof. P. Gao, Prof. Z. F. Liu  
Beijing Graphene Institute (BGI)  
Beijing 100095, China

B. Z. Liu, Prof. J. Y. Sun  
College of Energy  
Soochow Institute for Energy and Materials Innovations  
Jiangsu Provincial Key Laboratory for Advanced Carbon Materials  
and Wearable Energy Technologies  
Soochow University  
Suzhou 215006, China  
Prof. P. Gao  
Collaborative Innovation Center of Quantum Matter  
Beijing 100871, China

DOI: 10.1002/smll.202100098

eliminated at low temperatures, which, however, increases the difficulty for the decomposition of ammonia ( $\text{NH}_3$ ) and results in poor crystalline quality of the InGaN layer. Thus, new strategies are urgently needed to resolve these problems.

The process of In incorporation in InGaN alloys is closely related to its strain relaxation mechanism.<sup>[11]</sup> The stress release in the GaN template can effectively increase the incorporation of In in the subsequent InGaN layer. This is attributed to the suppression of phase separation and the reduced formation enthalpies of InGaN that promote the attainment of a fully relaxed strain state.<sup>[5]</sup> The van der Waals epitaxy (vdWE) of nitrides on the graphene (Gr) buffer layer is demonstrated to achieve low stress<sup>[12–14]</sup> and thus is expected to be valid for growth of In-rich InGaN at high temperatures by metal–organic chemical vapor deposition (MOCVD).<sup>[15,16]</sup> In this scenario, the requirement for the lattice match between the as-grown films and substrate is weakened due to the remote epitaxy mode,<sup>[17,18]</sup> resulting in the reduction of stress in the nitrides.<sup>[19–21]</sup>

In this study, a strain-modulated method is proposed to achieve the tunability of In incorporation in the InGaN layer. The epitaxy of high In composition on the light-emitting diode (LED) structure is achieved through Gr-nanorod (NR) enhanced quasi-vdWE. Remote epitaxy on the monolayer Gr/sapphire substrate results in the formation of an InGaN/GaN film with a highly consistent in-plane orientation due to the influence of the potential field of the substrate. Upon screening the covalent interaction of the substrate, the Gr layer is found to reduce the stress of the GaN film by 30%. Furthermore, by introducing a high-quality NRs buffer layer on the Gr, the stress of the GaN film is further reduced by 44.4%. As a result, the incorporation of In in the multiple quantum wells (MQWs) is significantly increased by 30.7%. Subsequently, the cyan LED device is fabricated and the photoelectric characteristics of the device are demonstrated. This work opens a feasible pathway for the

growth of high-quality In-rich InGaN alloys with tuned and ideal bandgaps under high temperatures for the fabrication of novel semiconductor devices.

## 2. Results and Discussion

Fabrication of the cyan LED device through Gr-NR enhanced quasi-vdWE is schematically shown in **Figure 1**. First, Gr synthesized by chemical vapor deposition (CVD) is transferred onto a c-plane sapphire substrate through wet corrosion and spatial transfer (Figure 1a).<sup>[22]</sup> Then, to promote the nucleation on Gr surface, AlGaN nucleation is deposited on the Gr/sapphire substrate (Figure 1b) due to the high adsorption energy and low migration barrier of Al adatoms.<sup>[23–26]</sup> Later GaN NRs are grown on it (Figure 1c). Finally, further growth of GaN NRs enables them coalesced to film (Figure 1d), on which epilayers including n-GaN, MQWs, and p-GaN (Figure 1e) are grown subsequently. After the procedures stated above, the layered LED structure could be formed as shown in Figure 1f from the cross-sectional view.

To relax the stress remained in the nitride epilayer on sapphire, we use two strategies, Gr-assisted quasi-vdWE and NRs. Monolayer Gr makes a great contribution for reducing lattice mismatch and thermal mismatch effect. In our attempts, high density GaN nanorods are formed at the energetically favorable edges of Gr domain boundaries and defect sites (Figure S1, Supporting Information). The sidewalls of hexagonal GaN NRs grown on monolayer Gr/sapphire are parallel to each other (Figure S2a, Supporting Information), while the hexagonal GaN NRs are angled to each other on the multilayer (four to five layers) Gr/sapphire (Figure S2b, Supporting Information). It is because that the sapphire under monolayer Gr could still guide the nitride layer growth by remote epitaxy,

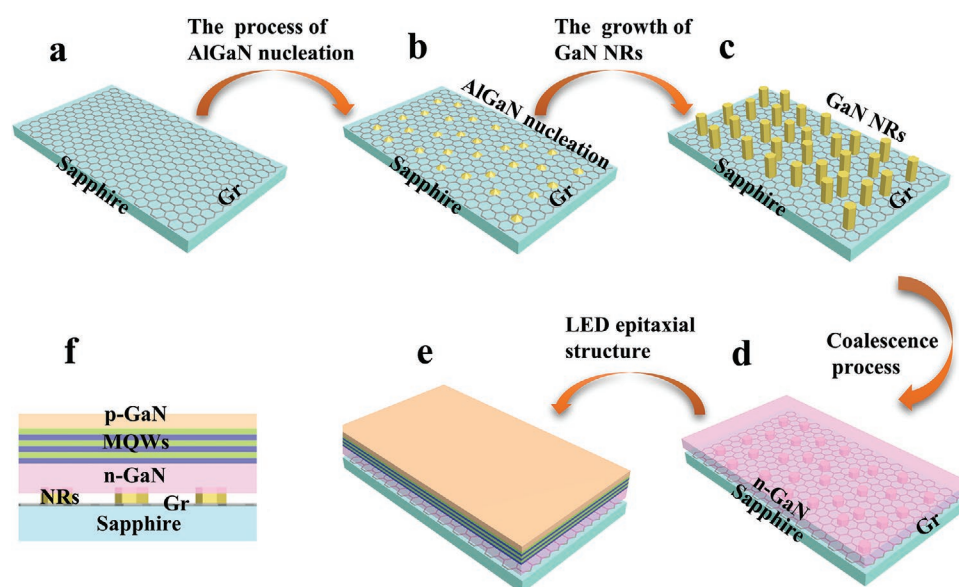


**Figure 1.** a) Transferred Gr on the sapphire substrate. b) AlGaN nucleation on Gr film. c) The evolution from AlGaN nucleation to GaN NRs. d) The step of coalescence to GaN film. e) Growth of subsequent epilayers including n-GaN, MQWs, and p-GaN. f) Cross-sectional view of the layered structure of LED.

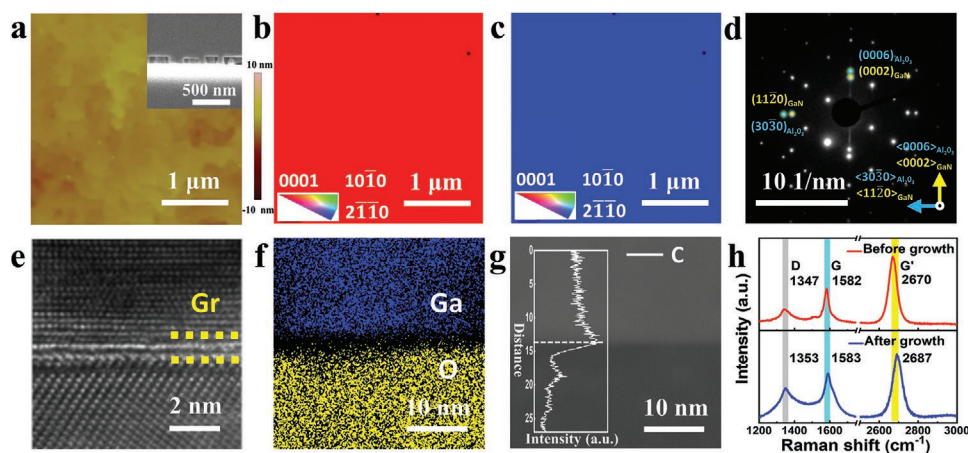


**Figure 2.** a) The AFM image of coalesced GaN film grown on monolayer Gr/sapphire substrate; the inset showing the cross-sectional SEM image of the gradient interface between GaN NRs and films. b) Normal-direction and c) transverse-direction EBSD IPF maps of as-grown GaN film. d) The SAED patterns from the interface of GaN/monolayer Gr/sapphire. The blue and yellow circles corresponding to sapphire and GaN, respectively. e) Cross-sectional HRTEM image of GaN/monolayer Gr/sapphire interface. f) The EDS mapping of Ga–O elements at the interface. g) The EDS linear scanning spectrum of C element at the interface. h) Raman spectra of monolayer Gr before (red) and after (blue) growth of GaN by MOCVD.

while the potential field of sapphire may be deadily damped through multilayer Gr.<sup>[17]</sup> As for this mechanism, the crystal lattice constants of Gr and GaN are not the main driving force of stress release. After the remote epitaxy through monolayer Gr, there can still be some residual stress in the GaN.<sup>[12,27]</sup> Therefore, NRs buffer layer is introduced to further release it. The GaN NRs with relatively high density could promote the coalescence process and reduce the critical coalesced thickness. The 2D growth dominating NRs coalescence process is carried out at a high V/III ratio condition in MOCVD and we finally obtain a continuous and smooth GaN film with the thickness of  $\approx 1.4 \mu\text{m}$  (Figure S3, Supporting Information). The root mean square roughness was measured as 0.53 nm by atomic force microscope (AFM) (Figure 2a). As a comparison, the GaN layer on multilayer Gr shows obvious crystal boundary and rough surface (Figure S4a, Supporting Information). The cross-sectional scanning electron microscopy (SEM) and transmission electron microscopy (TEM) images show the gradient interface between GaN NRs and film (inset of Figure 2a and Figure S4b, Supporting Information), from which the typical NRs exhibit an average diameter and height of 150 and 300 nm. Because of the nanoscale footprints on substrate, GaN NRs can reduce the stress accumulations, consequently suppressing the formation and propagation of dislocations during the coalescence process.<sup>[28]</sup> Therefore, NRs benefit the high-quality growth front and stress release for subsequent layers than other buffer strategies.<sup>[29–32]</sup>

The coalesced GaN film exhibits a highly c-oriented arrangement and consistent in-plane orientation from the normal-direction and transverse-direction electron backscatter diffraction (EBSD) inverse pole figure (IPF) maps (Figure 2b,c). High-resolution TEM (HRTEM) image, selected area electron diffraction (SAED) patterns, and X-ray diffraction (XRD)  $2\theta$ - $\omega$  spectrum further confirm the wurtzite structure and [0001] growth direction of GaN (Figure S5a–c, Supporting Information). The full width at half maximum of (0002) and (10 $\bar{1}2$ ) rocking curves from GaN film are 489 and 583 arcsec, respectively (Figure S5d,e, Supporting Information), which approximately correspond to

$4.81 \times 10^8$  and  $2.41 \times 10^9 \text{ cm}^{-2}$  for screw and edge dislocation densities in the coalesced GaN film.<sup>[33]</sup> The XRD phi scan and the arrangements of spots in SAED pattern from the GaN/monolayer Gr/sapphire interface (Figure S5f, Supporting Information, and Figure 2d) reveal that the epitaxial relationship between GaN and sapphire is defined as  $(0001)_{\text{GaN}} \parallel (0001)_{\text{sapphire}}$ ,  $[0\bar{1}10]_{\text{GaN}} \parallel [11\bar{2}0]_{\text{sapphire}}$ , which is consistent with the result of GaN growth directly on the sapphire substrate through the conventional two-steps method.<sup>[34]</sup>

After the epitaxy of GaN film, the cross-sectional HRTEM image of GaN/monolayer Gr/sapphire interface reveals the presence of the monolayer Gr at the interface (Figure 2e). The energy-dispersive X-ray spectroscopy (EDS) confirms the existence of monolayer Gr after epitaxial growth (Figure 2f,g). From the Raman spectra, the increased D peak intensity relative to the G peak intensity of Gr after growth indicates the introduction of defects in Gr during the epitaxy process, which could be attributed to the ammonia etching (Figure 2h).<sup>[35]</sup> Furthermore, the intensity ratio of G and G' peak is less than 1, corresponding to the characteristic of monolayer Gr.<sup>[36]</sup> The shift to higher frequencies of these peaks is attributed to nitridation and compressive strain of Gr during the MOCVD process.<sup>[37,38]</sup> According to the statements above, Gr-NR enhanced quasi-vdWE guarantees the crystal quality and epitaxial orientation of nitrides on the monolayer Gr/sapphire substrate.

The low strain environment benefits the In element incorporation. As shown schematically in Figure 3a, during the formation of InGaN epilayers, the In atom will replace a Ga atom and bond with three N atoms. Note that the position of N atoms bonded with In atom offsets the original position in the GaN lattice due to the large radius of In atom. When the stress of InGaN/GaN layer is released, the lattice matrix becomes larger and the stretching of In–N bonds gets weaker. Density functional theory (DFT) calculations are performed to verify the effects of stress state on In incorporation (Figure 3b). The results indicate that the formation enthalpies of InGaN substantially decreases as the lattice is gradually stretched, which could be understood by the fact that In atoms tend to

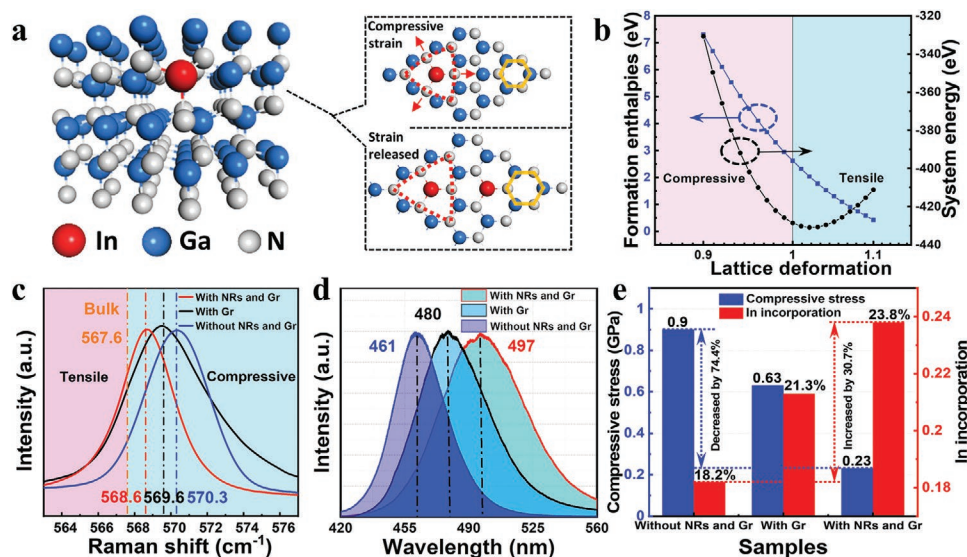


**Figure 3.** a) Atomic structures of In atoms incorporated into the GaN lattice matrix and that in compressive strain and released strain. b) Results of DFT calculations of InGaN formation enthalpies and system energy with lattice deformation. The blue plot showing that the formation enthalpies reduce significantly as the compressive stress decreases. The black plot representing the change in system energy. c) Raman spectra of GaN film, and d) PL spectra of the MQWs grown directly on sapphire (blue line), with monolayer Gr (black line), and with NRs and monolayer Gr (red line). e) The histograms of stress state in coalesced GaN film and In incorporation in InGaN/GaN MQWs on different substrates.

incorporate into a nitride matrix with a large lattice. The system energy of InGaN/GaN layer reaches the minimum when the system remains at a state of weak tensile stress, which is the most favorable for the incorporation of In.

The stress of GaN film is quantitatively investigated by Raman measurement (Figure 3c). The  $E_2$  mode peak in Raman spectra is strongly related to the biaxial stress in GaN film.<sup>[39,40]</sup> The peak position of GaN layer grown on pure sapphire (570.3 cm<sup>-1</sup>), monolayer Gr/sapphire without NRs (569.6 cm<sup>-1</sup>), and with NRs (568.6 cm<sup>-1</sup>) deviates from the characteristic frequency of unstrained GaN (568 cm<sup>-1</sup>),<sup>[41]</sup> suggesting that GaN layer subjects to a compressive strain. The deviation in frequency,  $\Delta\omega$ , compared with the stress-free bulk GaN could be estimated in terms of the biaxial stress,  $\sigma_{xx}$ , according to  $\Delta\omega = K\sigma_{xx}$ , where  $K$  is the linear stress coefficient (2.56 cm<sup>-1</sup> GPa<sup>-1</sup> for GaN).<sup>[40]</sup> The biaxial stress of GaN layer grown on pure sapphire, those grown with Gr and Gr-NRs are calculated as 0.9, 0.63, and 0.23 GPa, respectively, indicating that Gr reduces the stress of GaN film by 30%, and NRs further reduces it by 44.4%.

The MQWs structure is also grown and characterized to validate the results of In incorporation. The photoluminescence (PL) spectra peaks at 461 nm (without NRs and Gr), 480 nm (with Gr), and 497 nm (with NRs and Gr) correspond to the pumping of MQWs (Figure 3d). Compared to MQWs PL peak of the LED film grown directly on sapphire, those grown with Gr and Gr-NRs show large redshift, which is attributed to the effective In incorporation process during MOCVD growth when the compressive stress of coalesced film gets released through Gr-NR enhanced quasi-vdWE. Furthermore, the strong cyan lighting band and the absence of yellow band demonstrate the good functionality of MQWs and the high quality of the epilayers. According to NBE emission calculation and Vegard's law,<sup>[42,43]</sup> the In composition of InGaN QW grown on sapphire,

with Gr, and with NRs and Gr are calculated as 18.2%, 21.3%, and 23.8%, respectively. The stress state of coalesced GaN film and In incorporation in InGaN/GaN MQWs are summarized in Figure 3e. The stress is reduced by 74.4% and In incorporation in the MQWs is increased by 30.7% through Gr-NR enhanced quasi-vdWE.

The intense satellite peaks of InGaN/GaN MQWs in X-ray  $\omega$ -scan verify the high quality of MQWs grown on monolayer Gr/sapphire substrate through Gr-NR enhanced quasi-vdWE (Figure 4a). The EDS linear scanning spectrum along growth direction in MQWs implies that In composition gradually increases upward to sample surface and reaches a maximum in InGaN wells near the top layer (Figure 4b), which has good functionalities to realize the radiative recombination of electron and hole carriers. The In composition among metal elements in the sixth well from below is estimated to be 24.2% through EDS element analysis (Figure 4c), which is similar to the result calculated by PL measurement. Cross-sectional high angle annular dark-field (HAADF) scanning TEM (STEM) image and corresponding EDS images of In and Ga elements of MQWs show nine-period MQWs stripes with uniform distribution and no obvious In aggregations are observed (Figure 4b,d,e). Atomic-resolution STEM image of a single period InGaN/GaN heterostructure suggests that the d-spacing of InGaN and GaN are measured as 5.55 and 5.28 Å, respectively, and shows the ordered atomic arrangements with the growth direction along (0002) (Figure 4f). These results indicate the high-quality InGaN/GaN MQWs and uniform In composition distribution, which is an important prerequisite for the electrical and optical characteristics of the fabricated LED device.

The LED chips are fabricated through the conventional technological process. Figure 5a shows the schematic diagram of the as-fabricated LED structure through Gr-NR enhanced quasi-vdWE.  $I$ - $V$  characteristic of as-fabricated LED is obtained through chip-on-wafer measurements (Figure 5b). It

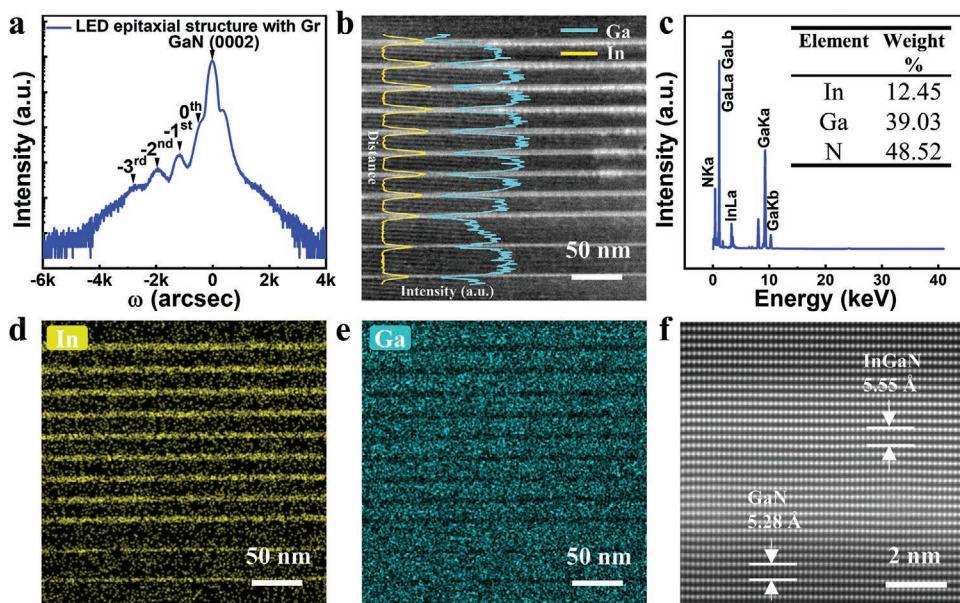


**Figure 4.** a) X-ray  $\omega$ -scan of InGaN/GaN MQWs grown on monolayer Gr/sapphire substrate through Gr-NR enhanced quasi-vdWE. b) HAADF STEM image of MQWs in the LED structure and the EDS linear scanning spectrum along growth direction in MQWs. c) The EDS element composition spectrum in InGaN well region. d,e) Corresponding EDS mapping of In and Ga elements in MQWs. f) Atomic-resolution STEM image of a period InGaN/GaN quantum well.

demonstrates a good rectification characteristic with a threshold voltage of 2.37 V (defined as the voltage value at 1 mA injection current) and a low leakage current of 0.31 mA at the bias

of  $-3$  V. The emitting photo of an as-fabricated LED in the inset of Figure 5b indicates a uniform cyan light distribution on the mesa of the LED chip at a 40 mA current. The parallel

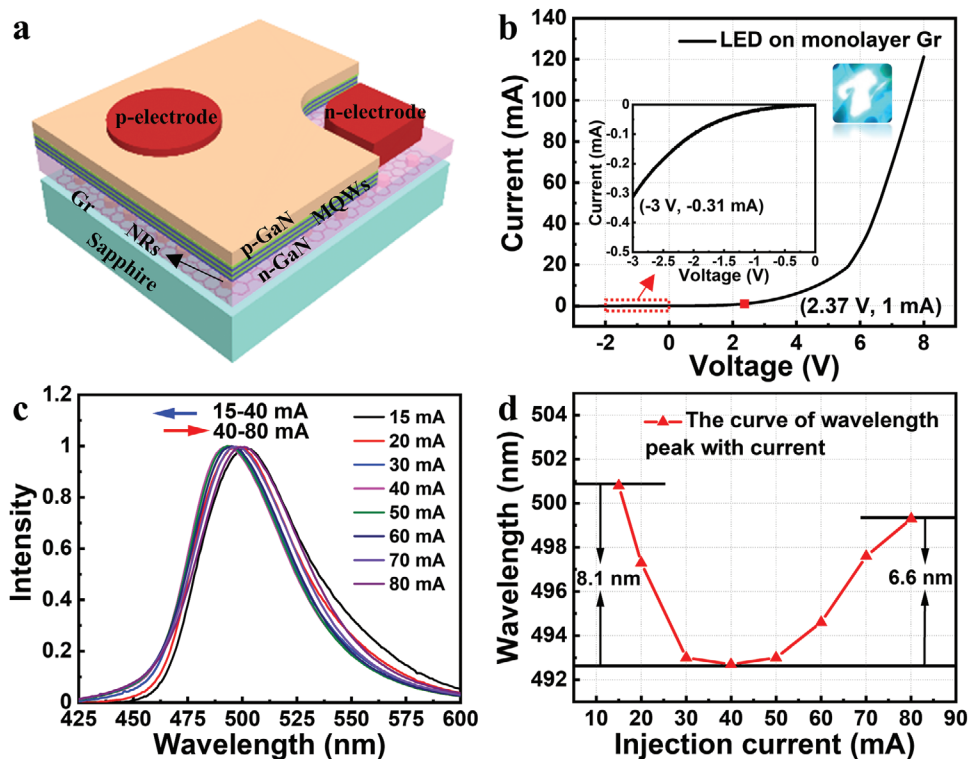


**Figure 5.** a) Schematic diagram of the as-fabricated LED structure. b)  $I$ - $V$  characteristic of as-fabricated LED grown on monolayer Gr; the insets are the amplified  $I$ - $V$  curve of LED working at inverse bias voltage and the picture of emitting LED at 40 mA current. c) EL spectra of an as-fabricated LED as a function of injection current. d) The wavelength peak shift of as-fabricated LED as a function of injection current.

resistance and series resistance are estimated to be 4.17 k $\Omega$  and 13.98  $\Omega$ , respectively (Figure S6, Supporting Information), indicating favorable crystalline quality and good Ohmic contact.<sup>[44]</sup> The normalized electroluminescence spectra confirm the light emission peaked at 493–501 nm (Figure 5c). The peak wavelength shows a blueshift and then a redshift, which is attributed to the band filling effect as well as the screening of charges effect, and bandgap decrease with increasing temperature, respectively.<sup>[45,46]</sup> These results demonstrate that the cyan LED structure with high-In-content is successfully fabricated on the monolayer Gr/sapphire substrate through Gr-NR enhanced quasi-vdWE and has compatibility with conventional industrial manufacturing processes like blue LED. Therefore, this technology provides a promising method for the functional application of Gr in longer wavelength LEDs.

### 3. Conclusion

In summary, an effective strain-modulated method, namely the Gr-NR enhanced quasi-vdWE, is demonstrated to overcome the fundamental limitations in the incorporation of In on the nitride epitaxy. The growth of In-rich InGa<sub>N</sub> film on a monolayer Gr/sapphire substrate and its application in long-wavelength LEDs are successfully achieved. The Gr acts as the transparent layer to sustain the epitaxial relationship through a remote epitaxy mechanism. Gr reduces the stress of the grown epilayers by 30%, and the NR layer further enhances the stress relief by 44.4%. As a result, the formation enthalpies of InGa<sub>N</sub> is substantially decreased, and the incorporation of In in the InGa<sub>N</sub>/Ga<sub>N</sub> MQWs is increased considerably by 30.7%. The PL peak of the MQWs exhibits a significant redshift of 36 nm. The fabricated LEDs on the Gr/sapphire substrate show cyan optical properties. This strategy can be used to achieve In-rich InGa<sub>N</sub> films with the expected high crystalline quality under high temperatures in the MOCVD process, which is compatible with conventional technology. These findings may expand the application of nitrides in novel devices based on high In composition such as nitride-based full-color displays and high-efficiency photovoltaic solar cells.

### 4. Experimental Section

**Transfer of Graphene:** The monolayer and multilayer Gr grown on Cu foil through CVD (Xicheng, Xiamen, China) were purchased commercially. The poly methyl-methacrylate (PMMA) was spin-cast onto the Gr-coated Cu foil at a 3000 rpm rate and then baked under 120 °C for 15 min. Subsequently, Cu foil was etched away in the FeCl<sub>3</sub> solution for  $\approx$ 3 h and the PMMA–Gr film was then floated on the surface owing to the surface tension. The PMMA-coated Gr was transferred onto the sapphire substrate and washed in deionized water to remove the FeCl<sub>3</sub>. Finally, acetone and ethanol were utilized to remove the PMMA.

**Epitaxial Growth of Nitride in Metal–Organic Chemical Vapor Deposition:** During the MOCVD growth process of nitride films, trimethylgallium (TMGa), trimethylaluminum (TMAI), and NH<sub>3</sub> were adopted as Ga, Al, and N precursor. Silane (SiH<sub>4</sub>) and magnesocene (Cp<sub>2</sub>Mg) were adopted as n-doped and p-doped source, respectively. Hydrogen (H<sub>2</sub>) acted as the carrier gas during the growth process. As for the nitride grown on Gr/sapphire substrate, the AlGa<sub>N</sub> nucleus was grown at a temperature of 1200 °C, with TMGa flow of 28 sccm, TMAI flow of 90 sccm, and NH<sub>3</sub> flow of 4000 sccm. Then, during the process of Ga<sub>N</sub> NRs growth and coalescence, the temperature was increased to 1250 °C, with the change

of NH<sub>3</sub> flow from 60 to 1500 sccm, and the TMGa flow was kept constant at 160 sccm for  $\approx$ 4800 s. As for the nitride directly grown on the sapphire substrate, the conventional two-steps growth was conducted. The low-temperature Ga<sub>N</sub> buffer layer was grown at 600 °C for 300 s with the NH<sub>3</sub> flow of 2800 sccm and the TMGa flow of 22 sccm. The u-GaN layer was grown at 1250 °C for 5400 s with the NH<sub>3</sub> flow of 2400 sccm and the TMGa flow of 80 sccm. The n-GaN layer of all samples was grown at 1250 °C for 4000 s, with SiH<sub>4</sub> flow of 12 sccm, the NH<sub>3</sub> flow of 2400 sccm, and the TMGa flow of 80 sccm, followed by nine periods of InGa<sub>N</sub>/Ga<sub>N</sub> layers grown at 720 °C/820 °C. Then, a p-GaN layer was deposited at 950 °C with the Cp<sub>2</sub>Mg flow of 120 sccm. The whole epilayers include the Gr/sapphire substrate, Ga<sub>N</sub> NRs, an n-GaN layer (1.6  $\mu$ m), nine-period In<sub>x</sub>Ga<sub>1-x</sub>N (5 nm)/Ga<sub>N</sub> (15 nm) MQWs, and a p-GaN layer (30 nm).

**Light-Emitting Diode Device Technological Process:** The LED devices were fabricated with 7  $\times$  9 mil<sup>2</sup> size using conventional mesa technology. An indium tin oxides (ITO) layer with a 280 nm thickness was deposited on the p-GaN layer to enhance the current spread through electron beam evaporation. The mesa (800 nm) was manufactured by photolithography and inductively coupled etching. Cr/Al/Ti/Au multilayer metal film was adopted as p- and n-type Ohmic contact electrodes through electron beam evaporation. Subsequently, the SiO<sub>2</sub> passivation layer was deposited to protect the chip through plasma-enhanced chemical vapor deposition. Finally, the wafer was sliced into chips and packaged.

**Characterization:** The as-grown nitride films were characterized by SEM (Hitachi, Tokyo, Japan; operated at 4.4 kV), XRD (Bede D1, United Kingdom; operated at 40 kV, 35 mA), PL microscopy (Horiba, Kyoto, Japan; 325 laser excitation), Raman microscopy (Horiba, Kyoto, Japan; Backscattering configuration; 532 nm linearly polarized laser excitation; Grating groove density of 1200 gr mm<sup>-1</sup>; focal length of 800 mm; spatial resolution of 2  $\mu$ m), TEM (JEM-F200) and STEM (FEI Titan Cubed Themis G2 300), both of which are equipped with EDS detectors, EBSD (Zeiss, Jena, Germany), and AFM (D3100, Veeco, New York, NY, USA). The as-fabricated LED device was measured by a source meter (Keithley 2400, USA) and an integrating sphere system (EVERFINE PHOTO-E-INFO Co., Ltd.).

### Supporting Information

Supporting Information is available from the Wiley Online Library or from the author.

### Acknowledgements

S.Z. and B.Y.L. contributed equally to this work. This research was funded by the National Key R&D Program of China (Grant Nos. 2018YFB0406603 and 2019YFA0708200), and the National Natural Science Foundation of China (Grant Nos. 61974140 and 61604140).

### Conflict of Interest

The authors declare no conflict of interest.

### Data Availability Statement

Research data are not shared.

### Keywords

graphene, high indium composition, quasi-van der Waals epitaxy, nitrides

Received: January 7, 2021  
Revised: February 21, 2021  
Published online: March 31, 2021

- [1] B. Nikoobakht, R. P. Hansen, Y. Zong, A. Agrawal, M. Shur, J. Tersoff, *Sci. Adv.* **2020**, 6, eaba4346.
- [2] H. Hu, B. Tang, H. Wan, H. Sun, S. Zhou, J. Dai, C. Chen, S. Liu, L. J. Guo, *Nano Energy* **2020**, 69, 104427.
- [3] F. Templier, *J. Soc. Inf. Disp.* **2016**, 24, 669.
- [4] J. W. Shon, J. Ohta, K. Ueno, A. Kobayashi, H. Fujioka, *Sci. Rep.* **2014**, 4, 5325.
- [5] A. M. Fischer, Y. O. Wei, F. A. Ponce, M. Moseley, B. Gunning, W. A. Doolittle, *Appl. Phys. Lett.* **2013**, 103, 131101.
- [6] C. A. M. Fabien, W. A. Doolittle, *Sol. Energy Mater. Sol. Cells* **2014**, 130, 354.
- [7] H. Liu, Z. Chen, S. Chu, X. Chen, M. Liu, N. Peng, G. Chu, F. Huang, R. Peng, *Adv. Opt. Mater.* **2017**, 5, 1700178.
- [8] J. Ju, B. Sun, G. Haunschild, B. Loitsch, B. Stoib, M. S. Brandt, M. Stutzmann, Y. K. Koh, G. Koblmüller, *AIP Adv.* **2016**, 6, 045216.
- [9] R. Singh, D. Doppalapudi, T. D. Moustakas, L. T. Romano, *Appl. Phys. Lett.* **1997**, 70, 1089.
- [10] Y. Abate, D. Seidlitz, A. Fali, S. Gamage, V. Babicheva, V. S. Yakovlev, M. I. Stockman, R. Collazo, D. Alden, N. Dietz, *ACS Appl. Mater. Interfaces* **2016**, 8, 23160.
- [11] F. Liu, Y. Yu, Y. Zhang, X. Rong, T. Wang, X. Zheng, B. Sheng, L. Yang, J. Wei, X. Wang, X. Li, X. Yang, F. Xu, Z. Qin, Z. Zhang, B. Shen, X. Wang, *Adv. Sci.* **2020**, 7, 2000917.
- [12] Z. Chen, X. Zhang, Z. Dou, T. Wei, Z. Liu, Y. Qi, H. Ci, Y. Wang, Y. Li, H. Chang, J. Yan, S. Yang, Y. Zhang, J. Wang, P. Gao, J. Li, Z. Liu, *Adv. Mater.* **2018**, 30, 1801608.
- [13] H. Chang, Z. Chen, W. Li, J. Yan, R. Hou, S. Yang, Z. Liu, G. Yuan, J. Wang, J. Li, P. Gao, T. Wei, *Appl. Phys. Lett.* **2019**, 114, 091107.
- [14] Z. Chen, Z. Liu, T. Wei, S. Yang, Z. Dou, Y. Wang, H. Ci, H. Chang, Y. Qi, J. Yan, J. Wang, Y. Zhang, P. Gao, J. Li, Z. Liu, *Adv. Mater.* **2019**, 31, 1807345.
- [15] M. I. Utama, Q. Zhang, J. Zhang, Y. Yuan, F. J. Belarre, J. Arbiol, Q. Xiong, *Nanoscale* **2013**, 5, 3570.
- [16] J. Kim, C. Bayram, H. Park, C.-W. Cheng, C. Dimitrakopoulos, J. A. Ott, K. B. Reuter, S. W. Bedell, D. K. Sadana, *Nat. Commun.* **2014**, 5, 4836.
- [17] Y. Kim, S. S. Cruz, K. Lee, B. O. Alawode, C. Choi, Y. Song, J. M. Johnson, C. Heidelberger, W. Kong, S. Choi, K. Qiao, I. Almansouri, E. A. Fitzgerald, J. Kong, A. M. Kolpak, J. Hwang, J. Kim, *Nature* **2017**, 544, 340.
- [18] W. Kong, H. Li, K. Qiao, Y. Kim, K. Lee, Y. Nie, D. Lee, T. Osadchy, R. J. Molnar, D. K. Gaskill, R. L. Myers-Ward, K. M. Daniels, Y. Zhang, S. Sundram, Y. Yu, S. H. Bae, S. Rajan, Y. Shao-Horn, K. Cho, A. Ougazzaden, J. C. Grossman, J. Kim, *Nat. Mater.* **2018**, 17, 999.
- [19] R. Huang, *Nat. Nanotechnol.* **2011**, 6, 537.
- [20] Y. Kobayashi, K. Kumakura, T. Akasaka, T. Makimoto, *Nature* **2012**, 484, 223.
- [21] C. H. Lee, Y. J. Kim, Y. J. Hong, S. R. Jeon, S. Bae, B. H. Hong, G. C. Yi, *Adv. Mater.* **2011**, 23, 4614.
- [22] F. Ren, Y. Yin, Y. Wang, Z. Liu, M. Liang, H. Ou, J. Ao, T. Wei, J. Yan, G. Yuan, X. Yi, J. Wang, J. Li, *Materials* **2018**, 11, 2372.
- [23] T. Löher, Y. Tomm, C. Pettenkofer, W. Jaegermann, *Appl. Phys. Lett.* **1994**, 65, 555.
- [24] P. Gupta, A. A. Rahman, N. Hatui, M. R. Gokhale, M. M. Deshmukh, A. Bhattacharya, *J. Cryst. Growth* **2013**, 372, 105.
- [25] S. Ruffenach-Clur, O. Briot, J. L. Rouvière, B. Gil, R. L. Aulombard, *Mater. Sci. Eng., B* **1997**, 50, 219.
- [26] W. Hong, H. N. Lee, M. Yoon, H. M. Christen, D. H. Lowndes, Z. Suo, Z. Zhang, *Phys. Rev. Lett.* **2005**, 95, 095501.
- [27] H. Ci, H. Chang, R. Wang, T. Wei, Y. Wang, Z. Chen, Y. Sun, Z. Dou, Z. Liu, J. Li, P. Gao, Z. Liu, *Adv. Mater.* **2019**, 31, 1901624.
- [28] B. H. Le, S. Zhao, X. Liu, S. Y. Woo, G. A. Botton, Z. Mi, *Adv. Mater.* **2016**, 28, 8446.
- [29] H. Yoo, K. Chung, Y. S. Choi, C. S. Kang, K. H. Oh, M. Kim, G. C. Yi, *Adv. Mater.* **2012**, 24, 515.
- [30] P. Gupta, A. A. Rahman, N. Hatui, J. B. Parmar, B. A. Chalke, R. D. Bapat, S. C. Purandare, M. M. Deshmukh, A. Bhattacharya, *Appl. Phys. Lett.* **2013**, 103, 181108.
- [31] Y. Xu, B. Cao, Z. Li, D. Cai, Y. Zhang, G. Ren, J. Wang, L. Shi, C. Wang, K. Xu, *ACS Appl. Mater. Interfaces* **2017**, 9, 44001.
- [32] K. Chung, H. Yoo, J. K. Hyun, H. Oh, Y. Tchoe, K. Lee, H. Baek, M. Kim, G.-C. Yi, *Adv. Mater.* **2016**, 28, 7688.
- [33] H. Heinke, V. Kirchner, S. Einfeldt, D. Hommel, *Appl. Phys. Lett.* **2000**, 77, 2145.
- [34] K. Hiramatsu, H. Amano, I. Akasaki, H. Kato, N. Koide, K. Manabe, *J. Cryst. Growth* **1991**, 107, 509.
- [35] A. C. Ferrari, J. C. Meyer, V. Scardaci, C. Casiraghi, M. Lazzeri, F. Mauri, S. Piscanec, D. Jiang, K. S. Novoselov, S. Roth, A. K. Geim, *Phys. Rev. Lett.* **2006**, 97, 187401.
- [36] Z. Chen, H. Ci, Z. Tan, Z. Dou, X.-d. Chen, B. Liu, R. Liu, L. Lin, L. Cui, P. Gao, H. Peng, Y. Zhang, Z. Liu, *Nano Res.* **2019**, 12, 1888.
- [37] Z. Zafar, Z. H. Ni, X. Wu, Z. X. Shi, H. Y. Nan, J. Bai, L. T. Sun, *Carbon* **2013**, 61, 57.
- [38] Z. Y. Al Balushi, T. Miyagi, Y.-C. Lin, K. Wang, L. Calderin, G. Bhimanapati, J. M. Redwing, J. A. Robinson, *Surf. Sci.* **2015**, 634, 81.
- [39] J. H. Ryu, Y. S. Katharria, H. Y. Kim, H. K. Kim, K. B. Ko, N. Han, J. H. Kang, Y. J. Park, E. K. Suh, C. H. Hong, *Appl. Phys. Lett.* **2012**, 100, 181904.
- [40] A. H. Park, T. H. Seo, S. Chandramohan, G. H. Lee, K. H. Min, S. Lee, M. J. Kim, Y. G. Hwang, E. K. Suh, *Nanoscale* **2015**, 7, 15099.
- [41] M. M. Muhammed, M. A. Roldan, Y. Yamashita, S. L. Sahonta, I. A. Ajia, K. Iizuka, A. Kuramata, C. J. Humphreys, I. S. Roqan, *Sci. Rep.* **2016**, 6, 29747.
- [42] K. Osamura, S. Naka, Y. Murakami, *J. Appl. Phys.* **1975**, 46, 3432.
- [43] Y.-K. Kuo, B.-T. Liou, S.-H. Yen, H.-Y. Chu, *Opt. Commun.* **2004**, 237, 363.
- [44] H.-W. Huang, C. C. Kao, J. T. Chu, H. C. Kuo, S. C. Wang, C. C. Yu, *IEEE Photonics Technol. Lett.* **2005**, 17, 983.
- [45] I. H. Brown, I. A. Pope, P. M. Smowton, P. Blood, J. D. Thomson, W. W. Chow, D. P. Bour, M. Kneissl, *Appl. Phys. Lett.* **2005**, 86, 131108.
- [46] J. Senawiratne, A. Chatterjee, T. Detchprohm, W. Zhao, Y. Li, M. Zhu, Y. Xia, X. Li, J. Plawsky, C. Wetzel, *Thin Solid Films* **2010**, 518, 1732.